Supporting Information

Giant field enhancements in ultrathin nanoslots above 1 terahertz

Dasom Kim,[1] Jeeyoon Jeong,[1] Geunchang Choi,[1] Young-Mi Bahk,[2] Taehee Kang,[1]

Dukhyung Lee,[1] Bidhek Thusa,[1] and Dai-Sik Kim[1*]

[1]Department of Physics and Astronomy and Center for Atom Scale Electromagnetism, Seoul National University, Seoul 08826, Korea

[2]Department of Physics, Incheon National University, Incheon 22012, Korea

*E-mail: dsk@phya.snu.ac.kr

1. Terahertz time domain spectroscopy

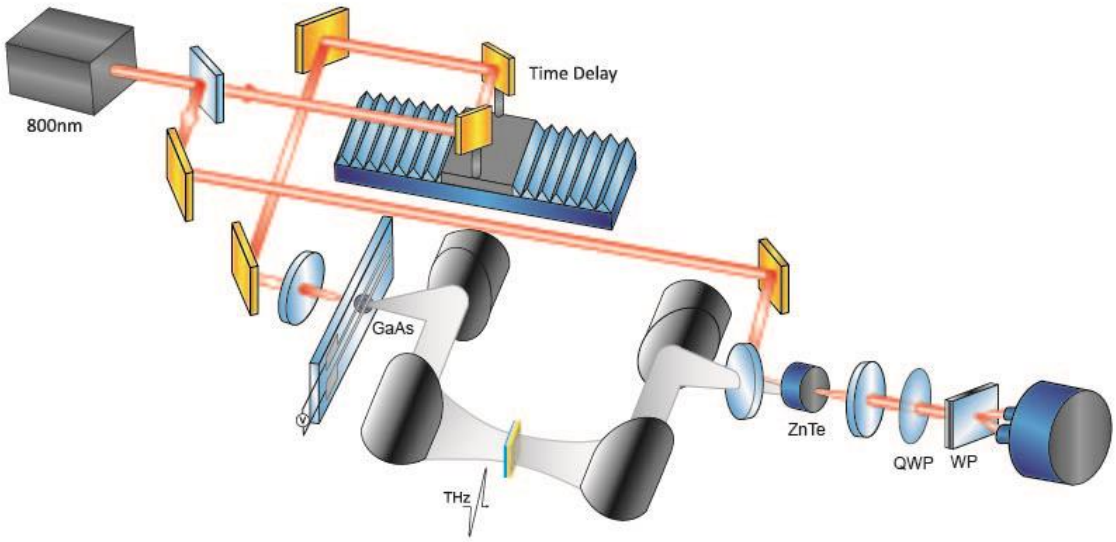

Figure S1 Experimental setup for THz-TDS consisting of GaAs emitter, nanoslots, and ZnTe electro-optic detector. A single-cycle terahertz source with maximum field strength of 30 V/cm is generated from photoconductive antenna. A biased semi-insulating GaAs emitter is illuminated by a 80 MHz repetition rate femtosecond Ti:Sapphire laser oscillator.[1] A 1mm thick <110> oriented ZnTe crystal detects transmitted terahertz field by electro-optic sampling.[2, 3] QWP is a quarter-wave plate, and WP is a Wollaston prism.

2. Near-field map near the nanogap

Commonly used three-dimensional (3D) modeling of electromagnetic waves such as FEM or FDTD method is very challenging for modeling of terahertz waves through the nanogaps, because of the large mismatch between wavelength and gap width ($\frac{w}{\lambda} \sim 10^5$) requiring enormous mesh elements and computational memories.[4] For these reasons, we simulate near-field distribution of terahertz waves in-plain and out-plan, separately.

A coaxial rectangular waveguide has lowest dipole mode as shown in Figure S2 (a). Electric field shows two sinusoidal distributions along the waveguide.[5] This mode is excited when the incident polarization is perpendicular to the slot as depicted in Figure S2 (b) and (c). Simulation results reveal that the rectangular waveguide effectively behaves as two identical rectangular slots. Also, the E_y field is excited in the slot but cancelled out in far-field because it has an antisymmetric field distribution. For these reasons, measured far-field transmissions are only attributed to the E_x field.[6]

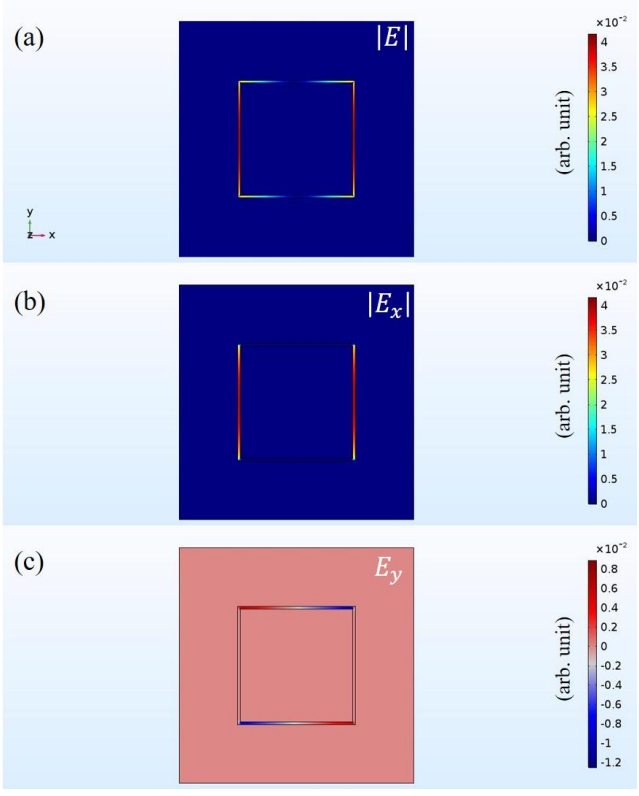

Figure S2 Top view of (a) the lowest dipole mode of a coaxial rectangular waveguide, (b) E_x, and (c) E_y. We simulate by COMSOL perfect electric conductor waveguide for briefly showing the near-field distributions at 1 THz. Rectangular waveguide has a length of 25 μm by 25 μm and a unit cell is 50 μm by 50 μm.

To show cross-sectional near-field distribution, we simulate infinitely long slits (Period = 25 μm) with gap width of 2 nm in a 180 and 10 nm-thick gold film. Figure S3 (a) and (b) respectively show the increased enhancement of a 180 and 10 nm thick gold film. They show the increased enhancement as gap thickness decreases. For the absence of resonance properties, they show field enhancement factors of 1400 and 160.

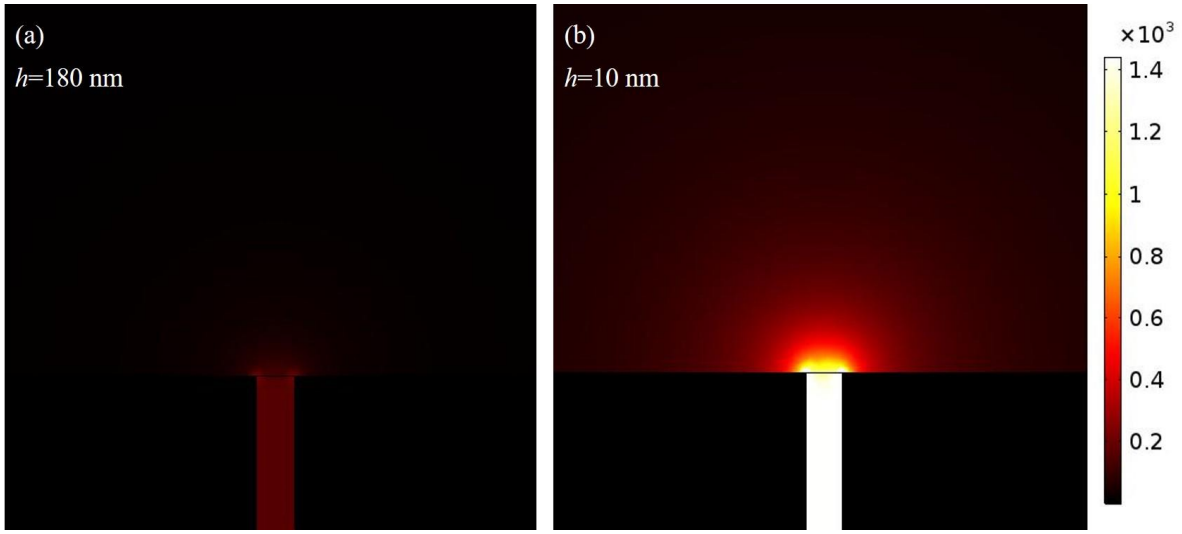

Figure S3 Cross-sectional view of calculated E_x field enhancement around 2 nm wide silt (a) in a 180 nm thick god film (b) in a 10 nm thick gold film on quartz at the frequency of 1.1 THz. Dielectric constant of gold is obtained from Drude model (plasma frequency of 1.37×10^4 THz, and damping parameter of 40.7 THz). Thickness dependent dielectric constant is used for alumina with refractive index of 1.73.[7] Field enhancements within the slot are normalized by a reference amplitude which propagates through the bare quartz.

3. Estimation of field enhancement using the Kirchhoff integral formalism

We measure far-field transmissions to estimate near-field enhancement factor using the Kirchhoff integral formalism, rather than directly measuring the near-field at the gap. Details of the calculation are represented by J. S. Kyoung et al..[8] Calculation geometry is as follows.

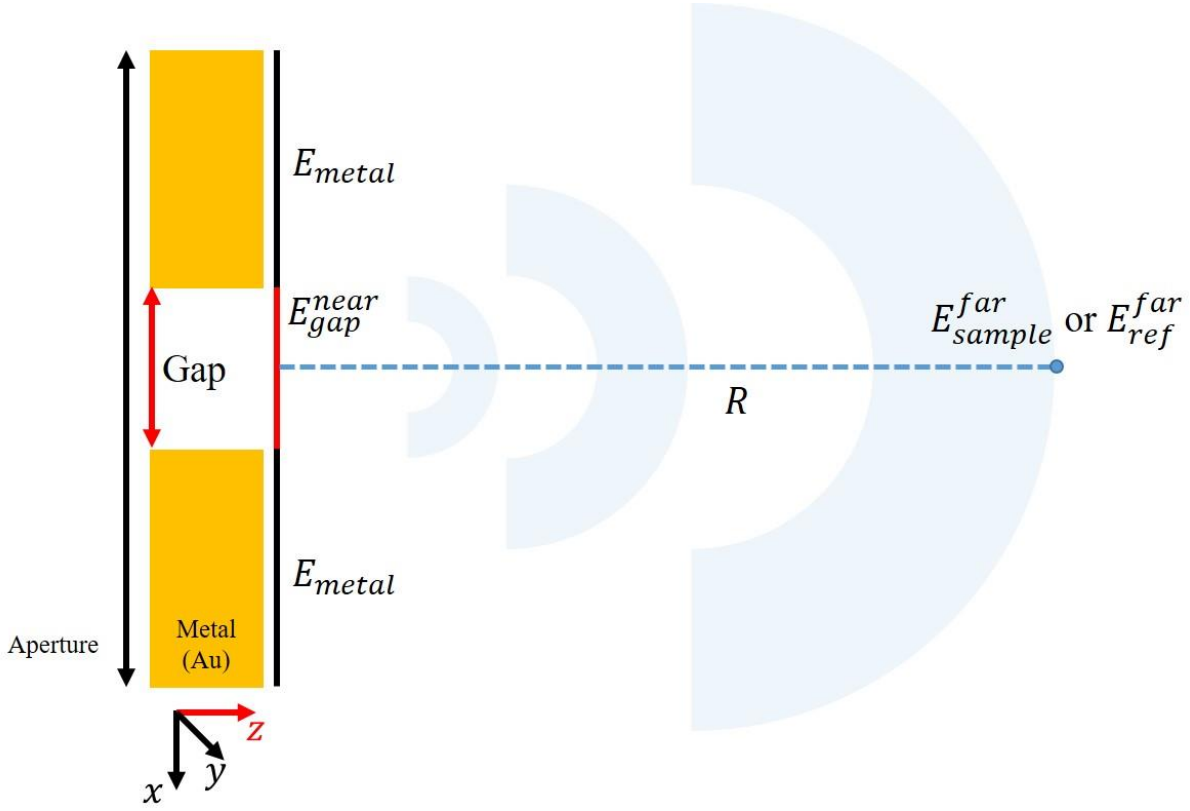

Figure S4 Calculation geometry and electric field around the nanogap.

The Kirchhoff integral formalism is based on the Green`s theorem[9] to express a field inside a closed volume *V* in terms of the values of the field and its normal derivative on the boundary surface *S*. Similarly, far-field transmissions which are obtained by our experiments are expressed in terms of integration of near-field at the gap, considering that direct transmission through the metal (E_{metal}) is negligible.

$$E_{sample}^{far} = \frac{e^{ikR}}{i\lambda R}\int E_{gap}^{near}\, dA_{gap}\,, \qquad E_{ref}^{far} = \frac{e^{ikR}}{i\lambda R}\int E_0\, dA_{aperture},$$

where A_{gap} and $A_{aperture}$ are respectively the area of the gap region and the aperture region in the unit cell. E_0 is an electric field amplitude after passing through the substrate. Note that direct transmission through the metal can be addressed by subtracting itself from E_{sample}^{far}. Considering that E_{sample}^{far} and E_{ref}^{far} are

experimentally obtained, the near-field enhancement is given by

$$\frac{E_{gap}^{near}}{E_0} = \frac{E_{sample}^{far}}{E_{ref}^{far}} \frac{A_{aperture}}{A_{gap}}.$$

Note that near-field enhancement factors present here are average values over the perpendicular-aligned slot to the incident wave. Therefore, a 2 nm wide slots (h = 10 nm) has a field enhancement factor of 0.303 * 50 μm *50 μm / (2 * 2 nm * 25 μm) = 7575, where the area of a unit cell is 50 μm *50 μm and a unit cell has two nanoslots.

4. Effect of tunneling on the field enhancement of the nanoslot

It is well-known that tunneling phenomena are important where the barrier size is down to nanometer. In order to reveal the quantum effects, we perform a power dependence experiment. In the main text, we estimate the electric field strength inside the nanoslot (h = 10 nm) as $13\ V/\mu m \approx FE(7600) * incident\ \ field(20\ V/cm) * \frac{4n}{(n+1)^2}(n = 2.1)$. Note that incident filed strength varies as a function of the frequencies as depicted in Figure S5 (a). We perform the experiment where the electric field strength inside the nanoslot as $8\ V/\mu m \approx FE(3000) * incident\ \ field(30\ V/cm) * \frac{4n}{(n+1)^2}(n = 2.1)$. Figure S5 (b) shows time-domain signal with different incident electric field strength and reveals almost the same results. Also, J. Y. Kim et al.[10] and K. J. Savage et al.[11] show that tunneling effect comes into play with the field strength of 1 V/nm in terahertz frequencies and 1 V/Å in optical frequencies. For these reasons, we estimate near-field enhancements without considering the quantum effects.

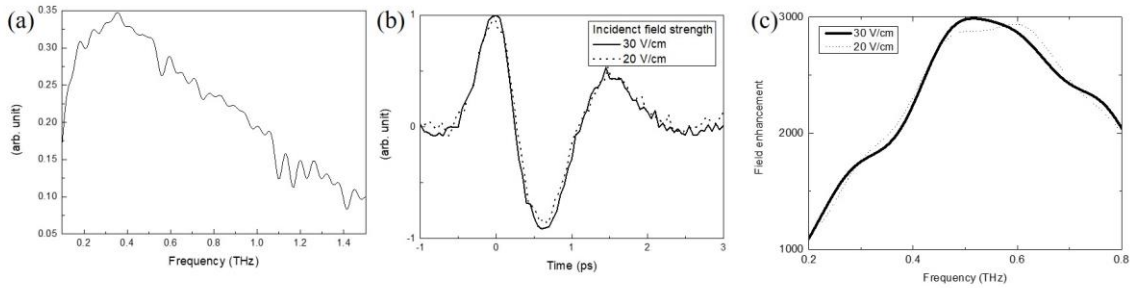

Figure S5 (a) Fourier transformed amplitude of the reference signal. (b) Transmitted time-domain signals with different incident electric field strength. (c) Field enhancements as a function of the frequencies with different incident electric field strength.

5. Transmitted amplitude of nanoslots

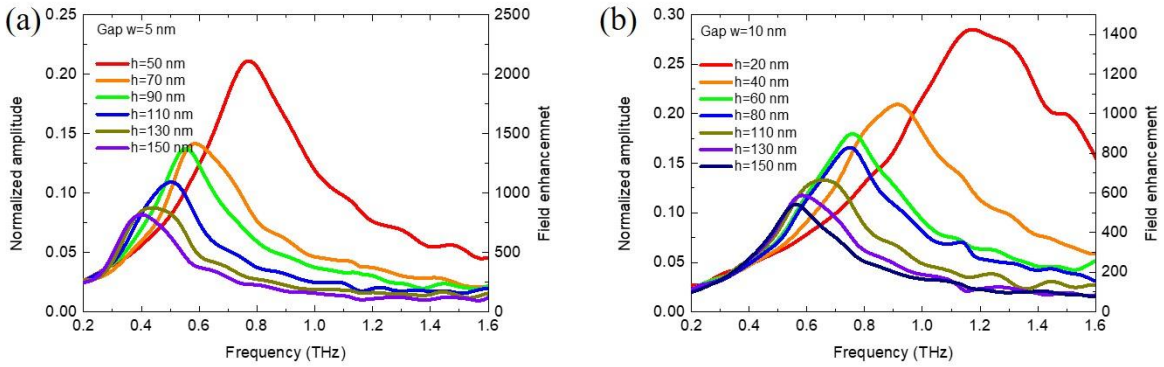

Figure S6 Experimental amplitudes and field enhancements normalized by the reference signal: (a) 5 nm wide slots, (b) 10 nm wide slots.

They show the increased enhancements as the metal thickness decreases. This tendency is identical to the results of 2 nm wide slots in the main text.

6. Calculation of field enhancement using modal expansion

We apply modal-expansion which assumes that electromagnetic modes inside the gap correspond with the waveguide modes of the gap.[12] This formalism still gives quasiexact results with the fundamental waveguide mode only.[13] Here, we apply the formalism of Garica-Vidal et al[12]. Our calculation combines the formalism of an array of rectangular slots in a real metal[14] and of effective index mode[15] which contains the effect of gap surface plasmon in terahertz regime. The effect of gap surface plasmon is expected to come into play since, ($\frac{w}{\lambda} \le \frac{\varepsilon_d}{\varepsilon_m}$), in the regime of our interest, where ε_m is the dielectric parameter of the metal[16] and ε_d is the dielectric constant of the material (Al_2O_3) inside the slots.[7] Although the thickness of the metal is thinner than skin-depth (~170 nm for 0.2 THz), direct transmission through the metal film of 10 nm is experimentally less than 3 %. The huge reflection on the front metal surface allows us to apply this formalism to our work.[17] By matching the electromagnetic fields at the interfaces, we obtain modal amplitudes of the electric field. Electric field at the input and output sides of the slots, E and E' are calculated by a set of two coupled linear equations:

$$(G^{I} - \Sigma)E - G_V E' = I_0$$
$$(G^{III} - \Sigma)E' - G_V E = 0.$$

Note that in the main text, we plot the electric field enhancements averaged over the perpendicular-aligned slot to the incident wave. The spatial maximum field enhancement factor inside the slot is represented as

$$E' = \frac{G_V I_0}{(G^{I} - \Sigma)(G^{III} - \Sigma) - G_V^2}$$ (at the center of the slot).[5]

The term I_0 represents the external illumination on the slot for normal incidence:

$$I_0 = \frac{i\sqrt{2}}{1 + Z_s} \frac{\frac{2l}{\pi}\sin(\frac{\pi l_2}{2l})}{\frac{l}{2\pi}\sin(\frac{\pi l_2}{l}) + \frac{l_2}{2}},$$

where $Z_s = \frac{1}{\sqrt{\varepsilon_m(\omega)}}$ is a surface impedance of the metal and l is half length of the rectangular ring, $l = l_x + l_y$.

The terms Σ and G_V are applied as presented in the previous work.[14] Electromagnetic coupling between the slots is controlled by the terms G^{I} and G^{III},

$$G^{I,III} = \sum_{m=-\infty}^{\infty}\sum_{n=-\infty}^{\infty} \frac{iwl}{d_x d_y} \frac{\varepsilon_{I,III} k_0 (k_0 + Z_s k_{Iz,IIIz}) - k_n^2}{(k_{Iz,IIIz} + Z_s k_0)(k_0 + Z_z k_{Iz,IIIz})} \mathrm{sinc}^2(\frac{wk_m}{2})[\mathrm{sinc}(\frac{lk_n + \pi}{2}) + \mathrm{sinc}(\frac{lk_n - \pi}{2})]^2,$$

with $k_{Iz,IIIz} = \sqrt{\varepsilon_{I,III} k_0^2 - k_m^2 - k_n^2}$, $k_m = \frac{2\pi m}{d_x}$, $k_n = \frac{2\pi n}{d_y}$, $k_0 = \frac{2\pi}{\lambda}$ (m and n are integer, $\varepsilon_{I,III}$ is the dielectric constants of the substrate and air, respectively). The admittance Y_{TE} and propagation constant of fundamental TE mode inside the slot q_z are replaced with the following expressions to consider the gap surface plasmon:

$$Y_{TE} = \frac{q_z}{k_0(1 + \frac{k_1^2}{\varepsilon_d k_0^2})}, \quad q_z = \sqrt{\varepsilon_d k_0^2 + k_1^2 - (\frac{\pi}{l})^2}$$

where, k_1 is the magnitude of the wave vector of the gap surface plasmon whose amplitude is given by[15] $k_1^2 = -\frac{1 + \sqrt{1 - 4k_0^2(\varepsilon_m - \varepsilon_d)(\frac{w\varepsilon_m}{2\varepsilon_d})^2}}{(\frac{\varepsilon_m}{\varepsilon_d})^2}$ giving an effective index of the gap $\tilde{n}_{2.eff} = n_{2.eff} + i\kappa_{2.eff} = \sqrt{\varepsilon_d + \frac{k_1^2}{k_0^2}}$. We now focus on the h dependence of the resonant field enhancement. E' becomes at resonance $E'_{res} \approx \frac{I_0}{\mathrm{Im}(G^I + G^{III} + Y_{TE} q_z h)}$ after using resonance condition presented in the next section. In case of w=150 nm ($k_1 = 0$), the last term in the denominator, $Y_{TE} q_z h = \frac{\varepsilon_d k_0^2 + k_1^2 - (\frac{\pi}{l})^2}{k_0(1 + \frac{k_1^2}{\varepsilon_d k_0^2})} h$, becomes an imaginary part of *zero* and also $\kappa_{2.eff} = \mathrm{Im}\left(\sqrt{\varepsilon_d + \frac{k_1^2}{k_0^2}}\right) = 0$. Therefore, $E'_{res} \approx \frac{I_0}{\mathrm{Im}(G^I + G^{III})}$, resonant field enhancement is almost identical for the small change of the propagation length with respect to the wavelength.

7. The comparative phase change compared with the reference pulse

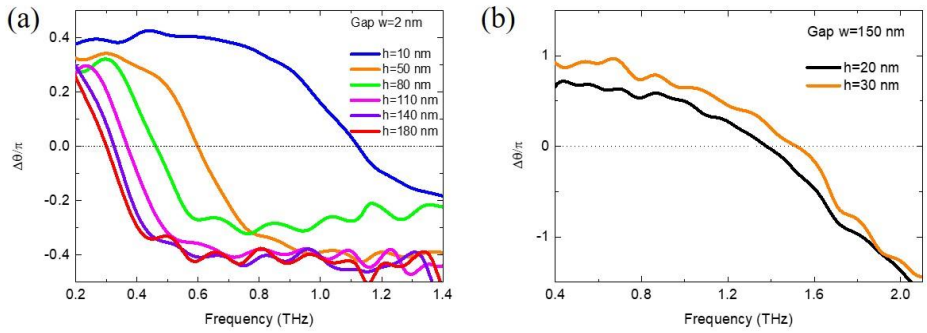

Figure S7 Experimental results of the phase change of (a) 2 nm wide slots and (b) 150 nm wide slots in radians.

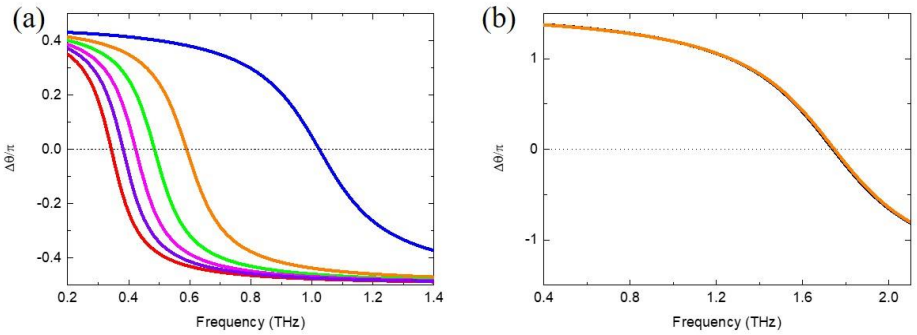

Figure S8 Corresponding theoretical calculations of the phase change of (a) 2 nm wide slots and (b) 150 nm wide slots in radians.

The resonance behavior occurs when the phase change is around the zero, in other words $\mathrm{Im}(E')=0$. Because I_0 is almost pure imaginary, the real part of the rest of the expression becomes zero. The characteristic equation is given by:

$$\mathrm{Re}(G^{I}+G^{III})\approx \mathrm{Re}(Y_{TE}q_z h).$$

For our case where the gap surface plasmon is dominant, after some algebra assuming $h\ll\lambda, \sqrt{\varepsilon_m}\sim 500(1+i)$, we obtain the following resonance frequency expression:

$$f_{res}\approx \frac{c_0/2l}{\sqrt{\varepsilon_a+\frac{\varepsilon_d h}{3w}}}.$$

References

(1) Grischkowsky, D.; Keiding, S.; van Exter, M.; Fattinger, C. Far-infrared time-domain spectroscopy with terahertz beams of dielectrics and semiconductors. *J. Opt. Soc. Am. B* **1990,** *7,* 2006-2015.

(2) Wu, Q.; Zhang, X. C. Free-space electro-optic sampling of terahertz beams. *Appl. Phys. Lett.* **1995,** *67,* 3523-3525.

(3) van der Valk, N. C. J.; Wenckebach, T.; Planken, P. C. M. Full mathematical description of electro-optic detection in optically isotropic crystals. *J. Opt. Soc. Am. B* **2004,** *21,* 622-631.

(4) Park, H.-R.; Chen, X.; Nguyen, N.-C.; Peraire, J.; Oh, S.-H. Nanogap-enhanced terahertz sensing of 1 nm thick (λ/106) dielectric films. *Acs Photonics* **2015,** *2,* 417-424.

(5) Jeong, J.; Kim, D.; Park, H.-R.; Kang, T.; Lee, D.; Kim, S.; Bahk, Y.-M.; Kim, D.-S. Anomalous extinction in index-matched terahertz nanogaps. *Nanophotonics* **2018,** *7,* 347-354.

(6) Chen, X.; Park, H.-R.; Pelton, M.; Piao, X.; Lindquist, N. C.; Im, H.; Kim, Y. J.; Ahn, J. S.; Ahn, K. J.; Park, N.; Kim, D.-S.; Oh, S.-H. Atomic layer lithography of wafer-scale nanogap arrays for extreme confinement of electromagnetic waves. *Nat. Commun.* **2013,** *4,* 2361.

(7) Groner, M. D.; Elam, J. W.; Fabreguette, F. H.; George, S. M. Electrical characterization of thin Al2O3 films grown by atomic layer deposition on silicon and various metal substrates. *Thin Solid Films* **2002,** *413,* 186-197.

(8) Kyoung, J.; Seo, M.; Park, H.; Ahn, K.; Kim, D. Far field detection of terahertz near field enhancement of sub-wavelength slits using Kirchhoff integral formalism. *Opt. Commun.* **2010,** *283,* 4907-4910.

(9) Jackson, J. D., *Classical electrodynamics*. 3rd ed.; Wiley: New York, 1999; p xxi, 808 p.

(10) Kim, J.-Y.; Kang, B. J.; Park, J.; Bahk, Y.-M.; Kim, W. T.; Rhie, J.; Jeon, H.; Rotermund, F.; Kim, D.-S. Terahertz Quantum Plasmonics of Nanoslot Antennas in Nonlinear Regime. *Nano Lett.* **2015,** *15,* 6683-6688.

(11) Savage, K. J.; Hawkeye, M. M.; Esteban, R.; Borisov, A. G.; Aizpurua, J.; Baumberg, J. J. Revealing the quantum regime in tunnelling plasmonics. *Nature* **2012,** *491,* 574.

(12) Garcia-Vidal, F. J.; Martin-Moreno, L.; Ebbesen, T.; Kuipers, L. Light passing through subwavelength apertures. *Rev. Mod. Phys.* **2010,** *82,* 729.

(13) Garcia-Vidal, F. J.; Moreno, E.; Porto, J. A.; Martin-Moreno, L. Transmission of light through a single rectangular hole. *Phys. Rev. Lett.* **2005,** *95*.

(14) Mary, A.; Rodrigo, S. G.; Martín-Moreno, L.; García-Vidal, F. J. Theory of light transmission through an array of rectangular holes. *Phys. Rev. B* **2007,** *76,* 195414.

(15) Gordon, R.; Brolo, A. G. Increased cut-off wavelength for a subwavelength hole in a real metal. *Opt. Express* **2005,** *13,* 1933-1938.

(16) Ordal, M. A.; Long, L. L.; Bell, R. J.; Bell, S. E.; Bell, R. R.; Alexander, R. W.; Ward, C. A. Optical properties of the metals Al, Co, Cu, Au, Fe, Pb, Ni, Pd, Pt, Ag, Ti, and W in the infrared and far infrared. *Appl. Opt.* **1983,** *22,* 1099-1119.

(17) León-Pérez, F. d.; Brucoli, G.; García-Vidal, F. J.; Martín-Moreno, L. Theory on the scattering of light and surface plasmon polaritons by arrays of holes and dimples in a metal film. *New J. Phys.* **2008,** *10,* 105017.